ELSEVIER

Journal of Molecular Catalysis A: Chemical 109 (1996) 239–248

JOURNAL OF MOLECULAR CATALYSIS A: CHEMICAL

ZrO_2–SiO_2 mixed oxides: surface aspects, photophysical properties and photoreactivity for 4-nitrophenol oxidation in aqueous phase

J.A. Navío [a,*], G. Colón [a], M. Macías [a], P.J. Sánchez-Soto [a], V. Augugliaro [b], L. Palmisano [b]

[a] *Instituto de Ciencias de Materiales, Centro Mixto Universidad de Sevilla and Departamento de Química Inorgánica, Facultad de Química, Universidad de Sevilla, E-41012 Sevilla, Spain*

[b] *Dipartimento di Ingegneria Chimica dei Processi e dei Materiali, Universitá di Palermo, Viale delle Scienze, 90128 Palermo, Italy*

Received 15 June 1995; accepted 1 December 1995

Abstract

Mixed oxides of ZrO_2 and SiO_2 were synthesized by a sol–gel technique by using zirconyl chloride and commercial silica gel as starting materials. The paper reports some surface features of the powders and the photoreactivity results obtained in the oxidation of 4-nitrophenol in aqueous suspensions of powdered photocatalyst. The optical characterization of the suspension was also performed by measuring the photon flows reflected and absorbed by the reacting system. The photoactivity exhibited by the ZrO_2–SiO_2 samples is very scarce especially if compared with that shown by a TiO_2 sample tested at equal experimental conditions. The low photoreactivity can be justified on the basis of two main reasons: (i) the unfavourable optical features of ZrO_2–SiO_2 suspensions in comparison with those of TiO_2 ones; and (ii) the lower degree of hydroxylation of ZrO_2–SiO_2 samples with respect to that of TiO_2 and, consequently, the less significant oxygen adsorption.

Keywords: Zirconia–silica; Photocatalysis; Photooxidation; Nitrophenol

1. Introduction

Zirconium dioxide, which is playing an important role in the field of high-technology ceramics [1], has also attracted considerable interest in the field of heterogeneous catalysis. The acid–base bifunctional properties of this oxide [2] allow its successful application to different catalytic processes such as paraffin isomerization [3], olefin hydrogenation [4], and alcohol dehydrogenation [5,6]. The preparation of ZrO_2-supported catalysts shows however some difficulties as the incorporation of ZrO_2 into a glass material has a significant influence on its properties. It has been shown [7,8] that the physical and chemical properties of ZrO_2 dispersed on SiO_2 matrix are different from those of bulk zirconia. Ishida et al. [9] have reported that the superacid properties obtained by homogeneously dispersing ZrO_2 on SiO_2 matrix can be correlated with the extent of crystallization.

Among the various catalytic processes, ZrO_2, due to its nature of n-type semiconducting oxide, has also been tested for performing photo-

* Corresponding author.

PII S1381-1169(96)00009-X

catalytic reactions; its photocatalytic activity has been successfully tested [10,11] although it has been well established that the photoactivity per unit surface area is far less than that shown by TiO_2 [10]. As the mixed catalysts show properties different from those of pure components, the addition of a foreign material to a semiconductor can change its photocatalytic properties by modifying, for example, the trapping or recombination centers [12]. For instance, Anpo, who investigated the photocatalytic activity of binary TiO_2–SiO_2 systems, reports [13] the enhancement of the photocatalytic activity of the TiO_2 moiety in the SiO_2 matrix in the region of lower Ti content. Similar studies on the photoactivity of the ZrO_2–SiO_2 system have not been performed; only recently, some surface characterizations of ZrO_2–SiO_2 powders prepared by a sol–gel method have been reported [8,14].

This paper reports the results of an investigation devoted to obtain a more thorough characterization of ZrO_2–SiO_2 powders. To this aim differential thermal and thermogravimetric analyses (DTA–TGA), temperature programmed desorption analysis in connection with mass spectrometry (TPD–MS), X-ray diffraction (XRD), BET surface areas determination and ultraviolet–visible diffuse reflectance spectroscopy (UV–Vis DRS) have been used. The photoactivity of the powders in aqueous suspensions has been also tested by performing the 4-nitrophenol oxidation as 'probe' photoreaction. The photon flows reflected and absorbed by the suspensions have been determined by using a method reported in the literature [15–17]. The photoactivity and the optical properties of ZrO_2–SiO_2 powders have been compared with those of a TiO_2 sample.

2. Experimental

2.1. Preparation of mixed oxides

The flow sheet of the mixed oxides preparation method is reported in Fig. 1. Various

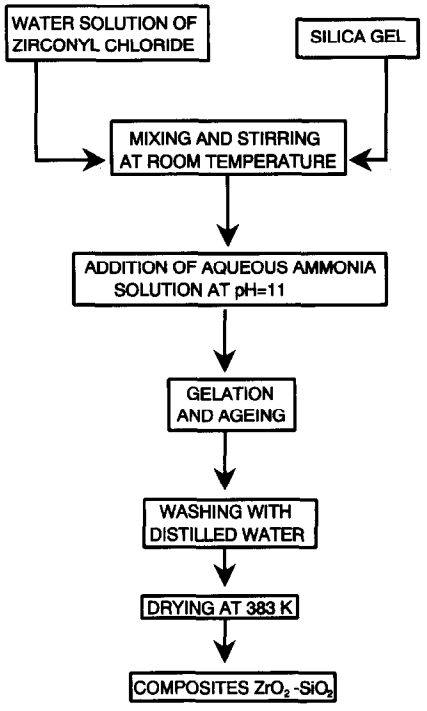

Fig. 1. Flow sheet of the preparation of the mixed oxides.

ZrO_2–SiO_2 samples have been prepared with a ZrO_2 content in the range 3–75 mol.%. The corresponding amounts of zirconyl chloride ($ZrOCl_2 \cdot 8H_2O$, Fluka AG, 43–44% ZrO_2) were deposited onto SiO_2 (Aldrich, Davisil silica gel 99%, grade 634, $S_{BET} = 410\ m^2 \cdot g^{-1}$) via sol–gel method using aqueous ammonia (Panreac, 28% by weight) at pH = 10–11.

After gelation the solids were filtered and repeatedly washed until $AgNO_3$ test was negative, thus assuring the absence of chloride ions in the samples. The samples were therefore dried overnight at 383 K and the resulting powders were then calcined at 1273 K for one or two hours.

2.2. Techniques

DTA–TGA spectra were simultaneously obtained in static air with a high temperature thermal analyzer (Setaram, model 92-16,18) at a heating rate of 8 $K \cdot min^{-1}$. About 40 mg of fine powdered samples were gently packed in a

10% platinum–rhodium holder of 100 μl total volume. Calcined alumina was used as reference sample. A furnace with inner graphite heating elements and alumina protection tubes was used for the samples thermal treatments.

BET surface areas were determined by using N_2 as adsorbate at 77 K with a Micromeritics Flowsorb 2200 apparatus.

X-ray diffraction spectra were obtained by using a Siemens D-501 diffractometer using Ni-filtered Cu Kα radiation.

TPD–MS experiments were performed under a helium flow of 100 $cm^3 \cdot min^{-1}$ by connecting the tube containing the sample to a Mass Spectrometer equipped with a quadrupole sensing head (Leybold, mod. QF-200) and a Faraday-cup detector. A heating rate of 8 $K \cdot min^{-1}$ was used for all the runs.

UV–Vis diffuse reflectance spectra were recorded by a spectrophotometer (Perkin Elmer, Lambda 9) using barium sulphate as reference sample.

2.3. Photoreactivity tests

Photoreactivity runs were carried out in a Pyrex annular batch photoreactor provided with a number of ports in its upper section for the passage of gasses, for sampling and for pH and temperature measurements. A 125 W medium pressure Hg lamp (Helios Italquartz) was positioned within the inner part of the photoreactor and cooling water was circulated through a Pyrex jacket surrounding the lamp. This arrangement allowed to avoid overheating and to cut off the IR component of the incident radiation as well as any radiation of wavelength below approximately 300 nm.

The photon flow emitted by the lamp in the 290–410 nm wavelength range was measured by a radiometer (Digital, UVX) leaned against the exterior wall of the photoreactor containing only distilled water; the incident photon flow was $\Phi_i = 7 \cdot 10^{-6}$ einstein $\cdot s^{-1}$.

The photoreactivity experiments were performed with an initial reaction volume of 500 cm^3 and lasted 4 h; at fixed intervals of time samples were withdrawn for analysis. During the runs oxygen at atmospheric pressure was continuously bubbled in the suspension that was stirred by means of a magnetic bar. The temperature of the reacting mixture was almost constant during the runs; its mean value was 300 ± 2 K. The initial pH of the suspension was 4.5 and was adjusted by using H_2SO_4 (Carlo Erba, RPE). The concentrations of the catalyst and of 4-nitrophenol were 4 and 0.05 $g \cdot l^{-1}$, respectively. At the experimental conditions used the photon flow transmitted by the suspension was about 1% of the incident one. Preliminarily to the photoreactivity runs, some blank tests were carried out or in the absence of radiation or by irradiating a suspension containing the silica used as support.

The 4-nitrophenol (BDH) was used as received; its quantitative determination [18] was performed by measuring its absorption at 315 nm, by using a UV–Vis spectrophotometer (Varian, DMS 90) after separation of the solid phase by filtration through a 0.45 μm cellulose acetate membrane (Millipore, HA).

For the sake of comparison a photoreactivity run was carried out by using TiO_2 (Degussa, P-25, crystalline phase: ca. 80% anatase, 20% rutile) instead of ZrO_2–SiO_2 photocatalyst; all the experimental conditions were previously reported but the powder concentration was of 1 $g \cdot l^{-1}$. At this TiO_2 concentration the transmitted photon flow was about 1% of the incident one. In this way the comparison between the ZrO_2–SiO_2 mixed samples and the TiO_2 was made at equal irradiation conditions.

2.4. Reflected and absorbed photon flow determination

The experimental apparatus for photon flow determination was made of two cylindrical vessels (i.d. = 58 mm) of Pyrex glass, vertically positioned one on top of the other. The upper vessel contained the aqueous suspension of the solids under investigation and the lower one an

appropriate ferrioxalate actinometer solution [19]. The external surfaces of both vessels were covered by mirror-polished aluminum sheets while a Pyrex sheet was placed on the top of the upper vessel. All the apparatus was kept inside a box of black internal walls in which an oxygen atmosphere was maintained.

The suspension was directly irradiated from the circular top surface of the upper vessel. The arc lamp supply (Oriel, 8530) was furnished by a 1000 W lamp (Hanovia, L5173) and by a system of collimating lenses. The distance between the lenses and the top of the suspension was 71 cm and the photon flow impinging on the suspension was $\Phi_i = 4.63 \cdot 10^{-7}$ einstein $\cdot$ s^{-1}. The rates of backward reflected photons, Φ_r, and of absorbed photons, Φ_a, were determined according to a reported method [15–17] which essentially consists in measuring the transmitted photon flow, Φ_0, as a function of the suspension volume. The following volumes of aqueous suspension were used: 40, 50, 60, 70, 75, and 80 cm^3. The powders under investigation were sieved in order to obtain samples with the following ranges of particle size: 45–90 and 90–125 μm. It was not possible to obtain samples of particles with larger sizes. The irradiation of the suspension lasted 30 s; these runs were carried out at 298 K by using a powder concentration of 1 g $\cdot$ l^{-1} in the presence of a 4-nitrophenol concentration of 0.05 g $\cdot$ l^{-1}. The pH of the suspension was 4.5 and was adjusted by adding H_2SO_4. During the runs the suspension and the actinometer solution were agitated by means of a magnetic stirrer. At the end of each run the absorbance of the actinometer solution was measured at the wavelength of 510 nm.

3. Results and discussion

3.1. Bulk and surface characterization

Fig. 2 depicts some DTA–TGA spectra obtained with selected silica–zirconia composite gel powders. All these samples were initially

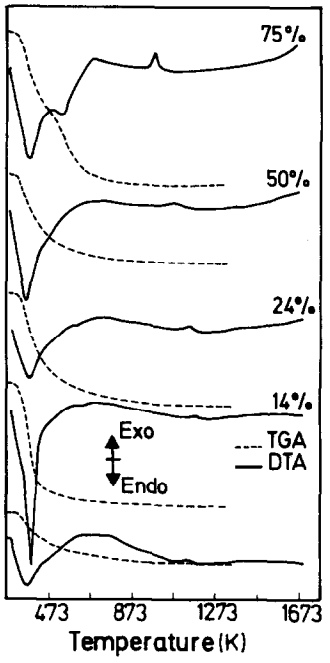

Fig. 2. DTA-TGA diagrams of ZrO_2–SiO_2 composite gel powders.

amorphous, as revealed by X-ray analysis. The broad endothermic peaks present in the DTA curves can be attributed to water desorption. MS analysis also showed that the evolved products are mainly water and traces of impurities such as residual ammonia. The differences, that can be observed in the DTA endothermic peaks of the zirconia–silica composite particles, are associated with distinct surface area and porosity parameters which are distinctly affected by the heat treatments.

Total weight losses are in the 15–30% range and they increase by increasing the zirconia content. Two different stages of weight loss appear at a zirconia molar content of 75%; this behaviour is in accord with the two endothermic peaks which appear in the DTA curves. These observations also agree with the TPD–MS analysis, as will be reported later. It is also remarkable to outline that the temperature of the endothermic peak of DTA curves decreases by decreasing the silica content in the composite core. This peak can likely be attributed to the

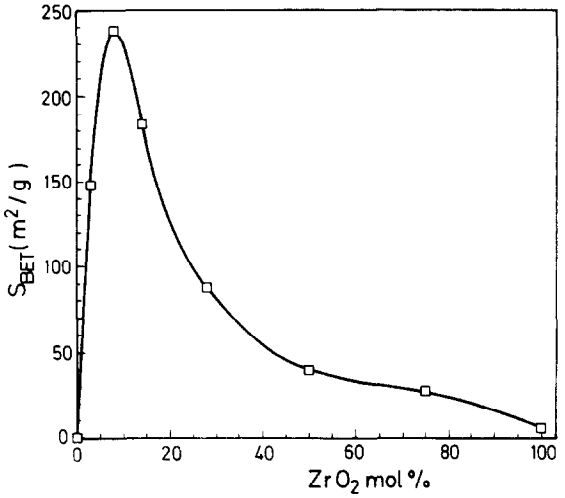

Fig. 3. Specific surface areas, S_{BET}, for ZrO_2–SiO_2 mixed oxides calcined at 1273 K for 1 h vs. ZrO_2 content.

zirconia crystallization in the metastable cubic-tetragonal phase.

As to particle morphology, two kinds of particles can be mainly inferred by considering the present results together with previously reported ones [14] obtained by the combined use of XPS, IR and EDAX techniques. In the region of lower zirconia content (less than 8% molar) it may be inferred the predominance of silica particles, which have few spots of zirconia or are partially (or totally) covered by zirconia. At higher contents of zirconia, instead, silica nuclei totally coated by zirconia and free zirconia particles are present, as revealed by SEM-EDAX analyses [7,14].

Fig. 3 shows the variation of the specific surface area with the ZrO_2 content in the binary ZrO_2–SiO_2 systems calcined at 1273 K for 1 h. On respect to this Figure it must be clarified that, although the S_{BET} of the commercial SiO_2 is equal to 410 $m^2 \cdot g^{-1}$, the calcination process performed on this sample determines a dramatic decrease of the surface area to ca. 1–2 $m^2 \cdot g^{-1}$, probably due to a sintering effect. From the observation of data reported in this Fig. 3, it may be noted that the surface area values are greatly affected by the ZrO_2 content in the SiO_2 matrix; they firstly increase by increasing the ZrO_2 content and achieve a maximum value for a ZrO_2 molar content of about 8%, which is the value corresponding to the likely formation of a monolayer of ZrO_2 on the SiO_2 matrix [20]. Beyond that ZrO_2 content the surface area values monotonically decrease.

In order to explain the dependence of BET surface area of ZrO_2–SiO_2 materials on the ZrO_2 content, the following model has been proposed [7]. Two different phenomena, which eventually have opposite effects on the surface area value, are contemporaneously occurring when ZrO_2 is added to SiO_2 at increasing amounts: (i) the interconnection among original silica particles by means of the precipitated amorphous zirconia, and (ii) the filling of silica pores. At low zirconia percentages (less than 8%) the addition of zirconia determines the aggregation of small particles into new larger ones and the partial filling of silica pores. When the resulting material is dried, owing to the relevant difference in the true densities of two oxides (SiO_2: $\rho \approx 2.3$ $g \cdot cm^{-3}$ and ZrO_2: $\rho \approx 5.6$ $g \cdot cm^{-3}$) a significant process of particles breaking occurs giving rise to small sub-particles partially coated by zirconia. In the range of higher zirconia contents the above mentioned process leads to small silica particles full and almost completely coated of zirconia together with free zirconia particles, as showed by SEM-EDAX analyses [7].

XRD spectra for a typical ZrO_2–SiO_2 sample heated at different temperatures are reported in Fig. 4. It may be noted that the thermal treatments at 573 and 673 K do not seem to affect the sample as it remains structurally amorphous as well as after heating at 1073 K. At about 1123 K an exothermic peak appears in DTA; however, the XRD analysis performed before and after the peak appearance shows that the crystallization process occurs without loss of weight. The spectrum recorded after a thermal treatment of the sample at 1273 K shows a crystalline structure of zirconia phase. It must be reported that pure ZrO_2 crystallizes in the monoclinic phase whereas the dispersion of zir-

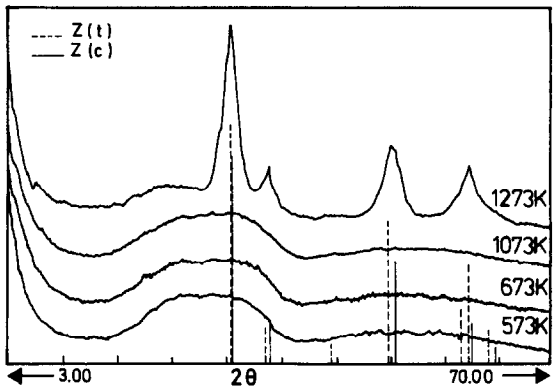

Fig. 4. Thermal evolution of ZrO_2–SiO_2 (24% molar of ZrO_2) as revealed by XRD. Z(t) = tetragonal ZrO_2; Z(c) = cubic ZrO_2.

conia onto the silica matrix leads to a mixed cubic-tetragonal crystalline phase, as shown by the XRD spectrum.

In Fig. 5 the water–TPD profiles of silica gel and crystalline zirconia (in monoclinic phase) are compared with those obtained when zirconia oxide in metastable cubic-tetragonal phase was dispersed onto SiO_2 matrix. Silica gel shows a narrow TPD peak centered at about 363 K and a slight continuous loss of water at temperatures above 523 K. Water desorption may be associated with molecular water adsorbed in open pores and with water molecules hydrogen-bonded to silanol groups [21].

For crystalline monoclinic ZrO_2 three desorption peaks, centered at 383, 523, and 673 K, respectively, are observed. These peaks can be attributed to different states of adsorbed water. The peak at 383 K may be assigned to desorption of physically adsorbed molecular water while those at 523 and 673 K can be attributed to chemically dissociated water molecules which eventually lead to the formation of Brønsted centers with basic (OH^-) and acidic (O^{2-}–H^+) nature.

TPD profiles for ZrO_2–SiO_2 mixed oxides calcined at 1273 K (spectra c–f of Fig. 5) show features completely different from those exhibited at lower temperatures. They present two main peaks, which are centered at 373 and 423 K and whose intensities increase by increasing the ZrO_2 content. This feature suggests, in accord with Yamaguchi et al. [22], that the basic hydroxyl groups of bulk ZrO_2 are disappearing to a considerable extent.

UV–Vis diffuse reflectance spectra of different composition ZrO_2–SiO_2 samples calcined for one hour at 1273 K are reported in Fig. 6. The mixed oxides show an increased absorbance with respect to pure SiO_2. The absorbances also increase by increasing the ZrO_2 content; a sample with a 75% molar content of ZrO_2 shows a spectrum very similar to that recorded for pure (monoclinic) ZrO_2. For all the

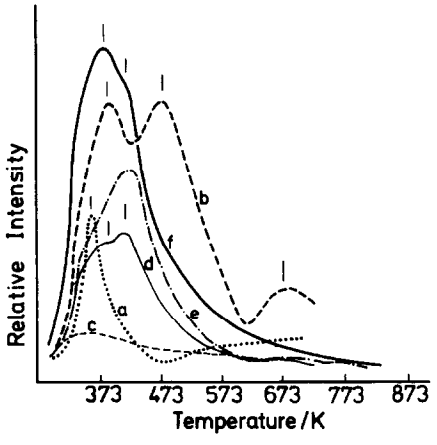

Fig. 5. H_2O-TPD profiles of: pure SiO_2 (a); pure ZrO_2 after calcination at 1273 K for 1 h (b); ZrO_2–SiO_2 binary oxides calcined at 1273 K for 1 h with a ZrO_2 molar percentage of 3 (c), 8 (d), 14 (e) and 75 (f).

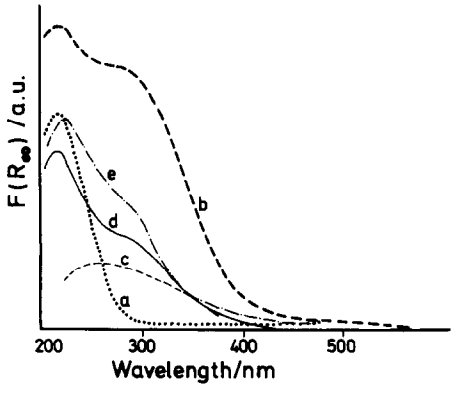

Fig. 6. UV–Vis DR spectra of samples (a) SiO_2; (b) the prepared ZrO_2 after calcination at 1273 K for 1 h, and binary oxides calcined at 1273 K for 1 h with a ZrO_2 molar percentage of 8 (c), 14 (d) and 75 (e).

mixed oxides the spectra are dominated by an absorption band close to 300 nm associated to a $[O^{2-} \rightarrow Zr^{4+}]$ charge transfer process. It is worth noting that in the ZrO_2–SiO_2 binary systems, the wavelength at which the maximum absorption peak is localized (around 300 nm) shifts towards shorter wavelengths by decreasing the zirconia content.

From the UV–Vis experimental spectra the values of the band-gap, E_g, have been determined according to the method proposed by Tandon and Gupta [23]. The following values have been obtained: $[SiO_2] = 4.5$ eV; $[ZrO_2] = 3.0$ eV; $[ZrO_2$–$SiO_2] = 3.1$, 3.4, and 3.5 eV for ZrO_2 molar percentages of 8, 14, and 75, respectively. The variation of the band-gap width between pure zirconia and zirconia dispersed on silica matrix is of about 0.3 ± 0.2 eV. This blue shift is quite significant and may be attributed to the quantum confinement effect; this phenomenon is frequent and well known in sulphides and selenides [24] while it is not common in oxides.

3.2. Photoreactivity

No reactivity was observed in the absence of light and/or of catalyst and/or of oxygen. The 4-nitrophenol concentration was found constant for the runs performed by irradiating pure silica; these runs lasted 6 h and they indicate the absence of 4-nitrophenol stripping from the solution due to the bubbling oxygen.

Figs. 7 and 8 report some experimental results of photoreactivity as 4-nitrophenol concentration versus the irradiation time for different powders. The following specimens were tested: (i) pure ZrO_2 heated for 1 or 2 hours at 1273 K; ZrO_2–SiO_2 with ZrO_2 molar percentages of 3, 14, and 75 heated for 2 h at 1273 K; ZrO_2–SiO_2 with ZrO_2 molar percentages of 8, 14, and 24 heated for 1 hour at 1273 K; ZrO_2–SiO_2 with a ZrO_2 molar percentage of 14 heated for 1 h at 573 K; ZrO_2–SiO_2 with a ZrO_2 molar percentages of 14 heated for 12 h at 383 K; and pure TiO_2 (Degussa, P-25).

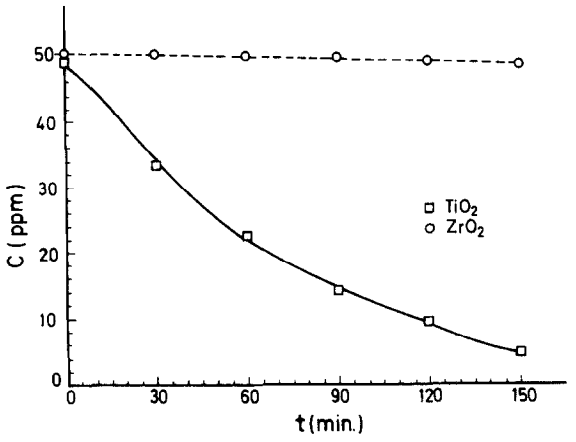

Fig. 7. Photoreactivity results as 4-nitrophenol concentration, c, vs. irradiation time, t, for different photocatalysts. Symbols: □, TiO_2 (Degussa, P-25); and ○, pure ZrO_2.

The photoactivity was low in the case of pure ZrO_2 and of the ZrO_2–SiO_2 samples. In the duration of the photoreactivity runs only few percentage units of conversion were reached; on the contrary, in the case of TiO_2 the almost complete photodegradation of 4-nitrophenol was achieved, in accord with literature data [18].

For all the runs the oxidation process exhibited a pseudo-first order kinetics with respect to the organic concentration; the values of the pseudo-first order rate constant, k_{obs}, were very small and they ranged from about $1.2 \cdot 10^{-4}$ to

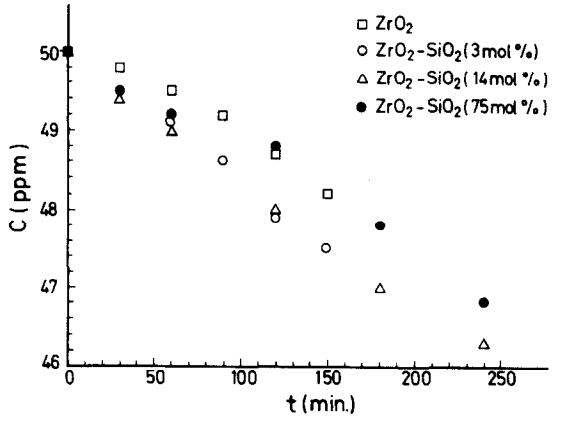

Fig. 8. Photoreactivity results as 4-nitrophenol concentration, c, vs. irradiation time, t, for different photocatalysts. Symbols: □, ZrO_2; ○, ZrO_2–SiO_2 (3% molar of ZrO_2); △, ZrO_2–SiO_2 (14% molar of ZrO_2); and ●, ZrO_2–SiO_2 (75% molar of ZrO_2).

$3.5 \cdot 10^{-4}$ min^{-1}. When TiO_2 was used in similar experimental conditions, the value of k_{obs} was $1.5 \cdot 10^{-2}$ min^{-1}. It must be outlined that the concentration of mixed oxide catalyst was four times higher than that of TiO_2 in order to obtain a negligible photon flow transmitted (and therefore lost) by the suspension during the experiments. It must be noted that the k_{obs} values here reported have no general applicability as they strongly depend on the particular features of the used system. They are utilized in the present work only for quantitatively comparing the performances of the powders at equal operative conditions.

It is well known that the photoreactivity depends on several factors as for instance the band-gap of the semiconductor, the energy levels of the conduction and valence bands, the Fermi level, the recombination rate of the photoproduced electron–hole pairs, the surface hydroxylation, the surface acid–base properties, the surface areas, the porosity, the amount of radiation absorbed by the suspension, etc. In particular, the photon absorption and reflection rates are important parameters needed for a general picture of the powders under investigation. To date scarce attention has been devoted to the determination of the above parameters as it is very difficult to experimentally measure them in aqueous suspensions. The method recently reported in the literature [15–17] and applied in this work allows to overcome this difficulty.

It is worth reporting that diaggregation of particles in water with formation of a milky suspension significantly occurred only for the TiO_2 sample. Pure ZrO_2 and ZrO_2–SiO_2 samples consisted of very tough particles and no evidence of milky aqueous suspension was found even during the suspension stirring. Consequently, the liquid–solid separation procedure was very easy. The mechanical resistance of mixed oxides is a very good feature of these materials; the main drawback is, however, that the k_{obs} values are two order of magnitude less than those of the TiO_2 sample tested in the present work and of other TiO_2 samples reported in the literature [18].

3.3. Photophysical properties

In Table 1 the backward reflected photon flows are reported as percentages of the impinging photon flow for ZrO_2 and for some representative ZrO_2–SiO_2 samples for particles in the 45–90 and 90–125 μm size ranges. No significant differences may be noted among the various samples and between the two different ranges of particle size. The mean value of the percentage of reflection is of about 60. The percentage of backward reflected photon flow is an intrinsic property of the material under inves-

Table 1
Backward reflected photon flows as percentage of the incident photon flow, R_B, and pseudo-first order rate constant, k_{obs}, for pure ZrO_2 and for ZrO_2–SiO_2 samples of different particle size

ZrO_2	1 h at 1273 K			2 h at 1273 K			1 h at 573 K	12 h at 383 K
mol.%	R_B (%)		$k_{obs} \cdot 10^4$ (min^{-1})	R_B (%)		$k_{obs} \cdot 10^4$ (min^{-1})	$k_{obs} \cdot 10^4$ (min^{-1})	$k_{obs} \cdot 10^4$ (min^{-1})
	45–90 μm	90–125 μm	45–125 μm	45–90 μm	90–125 μm	45–125 μm	45–125 μm	45–125 μm
100	60	61	2.4	–	–	2.3	–	–
75	70	67	–	62	62	2.6	–	–
24	55	55	1.9	–	–	–	–	–
14	71	69	1.2	–	–	3.2	1.4	1.8
8	62	66	–	–	–	–	–	–
3	69	66	–	–	–	3.8	–	–
0	76	75	–	–	–	–	–	–

tigation, as it has been reported for TiO_2 specimens [25,26]; consequently, it is understandable why there are not significant differences between the two ranges of particle size. The similarities of percentage values among the different samples containing different amount of ZrO_2 may be explained by taking into account that the preparation method of ZrO_2–SiO_2 mixtures does not produce particles of homogeneous composition but, on the contrary, particles in which ZrO_2 is preferentially located on the outer surface of SiO_2 grain. EDAX analyses, which determined the composition of a superficial skin of 1–2 μm depth, revealed zirconia molar ratio values higher than the nominal ones [14]. As a consequence, the optical features of ZrO_2–SiO_2 mixtures are predominantly determined by the ZrO_2 present on the surface. In experimental conditions similar to those used in this work, for TiO_2 aqueous suspension the percentage of reflected photon flow was in the 25–30% range.

Table 2 reports some representative results of the rate of photon absorption as percentages on the incident photon flow for the two particle size ranges used. It may be noted that the rate of photon absorption increases by increasing the content of ZrO_2 and reaches a maximum value for pure ZrO_2. In the case of TiO_2 aqueous suspensions in similar experimental conditions [25,26] the percentages of photon absorption were significantly higher, about 50–60%, than those obtained in the present work. Finally the photon absorption seems to increase by decreasing the particle size, at least for high contents of zirconia.

Table 2
Absorbed photon flows as percentage of the incident photon flow for pure ZrO_2 and for some representative ZrO_2–SiO_2 samples of different particle size ranges. Data are relative to a suspension volume of 75 cm^3

ZrO_2	Particle size	
mol.%	45–90 μm	90–125 μm
100	24	20
75	22	14
24	18	16
14	15	15
8	10	13
3	8	12
0	4	6

4. Concluding remarks

As mentioned before, the physical and chemical properties of zirconia dispersed on silica surface are different from those of pure zirconia. In the present investigation it has been found that ZrO_2–SiO_2 mixed oxides have a lower amount of acid and basic hydroxyl groups than pure ZrO_2 samples, as revealed by TPD–MS results; moreover, pure ZrO_2 crystallizes in the monoclinic phase whereas the dispersion of zirconia onto the silica matrix leads to a cubic-tetragonal crystalline phase. If the important role that hydroxyl groups play in the photoactivity of semiconductor materials is taken into account, it could be forecast a higher photoactivity of pure zirconia specimens with respect to that of zirconia–silica samples. The photoreactivity results reported in Table 1, however, show that there are not substantial differences in the photocatalytic activity between pure zirconia and the mixed oxides.

As to concern the spectral characteristics of the zirconia samples used in this work, it is worth to notice that the dispersion of zirconia oxide onto the silica matrix has a significant effect on the absorption properties of pure zirconia; however the very scarce and similar photoreactivity exhibited by pure zirconia and zirconia–silica samples can not be explained only in terms of the differences in the absorption spectra. It is well known [27] that TiO_2 presents an absorption edge located at 408 nm (3.04 eV) and a charge transfer band with a maximum at 325 nm; therefore the TiO_2 spectrum resembles that of our home prepared ZrO_2. However the photoreactivity exhibited by the zirconia specimen for the oxidation of 4-nitrophenol is very

scarce if compared with that of TiO_2. It is quite difficult to explain why TiO_2 is much more active photocatalyst than ZrO_2 of comparable band-gap [28]. It must be considered, however, that the identity of the photocatalyst strongly affects not only the band positions and hence the interfacial electron transfer energetics but also the absorption sites (nature and number), the surface charge, the adsorption equilibria, the density of surface states and traps and the rates of electron–hole recombination. It has been reported [10] that photoassisted oxygen isotope exchange over TiO_2 occurs at much higher rate than over ZrO_2 and similar conclusions may be drawn from photoconductance measurements.

Tentative explanations for the less significant photoactivity of zirconia (supported or mixed with silica gel) compared with that of TiO_2 could be: (i) its lower degree of hydroxylation and consequently the less significant oxygen adsorption; and (ii) its unfavourable photophysical features as the percentages of absorbed photon flow are quite lower for ZrO_2–SiO_2 suspensions than for TiO_2 suspensions.

Acknowledgements

JAN thanks the 'Dirección General de Investigación Científica y Técnica' (PB93-0917 DGICYT, Madrid) for supporting part of this work. VA and LP thank the 'Ministero dell'Universitá e della Ricerca Scientifica e Tecnologica' (MURST, Rome) for financial support.

References

[1] D.A. Ward and E.I. Ko, Chem. Mater., 5 (1993) 956.
[2] B.Q. Xu, T. Yamaguchi and K. Tanabe, Chem. Lett., (1989) 149.
[3] M. Hino, S. Kobayashi and K. Arata, J. Am. Chem. Soc., 101 (1979) 6439.
[4] T. Yamaguchi and J. Hightower, J. Am. Chem. Soc., 99 (1977) 4201.
[5] M.E. Winfield, in P.H. Emmett (Ed.), Catalysis, Vol. 7, Reinhold, New York, 1960, p. 93.
[6] T. Yamaguchi, H. Sasaki and K. Tanabe, Chem. Lett. (1973) 1017.
[7] J.A. Navío, F.J. Marchena, M. Macías and P.J. Sánchez-Soto, in P. Vincenzini (Ed.), Ceramics Today – Tomorrow's Ceramics, Materials Science Monographs, Vol. 66B, Elsevier, Amsterdam, 1991, p. 889.
[8] J.A. Navío, M. Macías, G. Colón and P.J. Sánchez-Soto, Appl. Surf. Sci., 70/71 (1993) 226.
[9] T. Ishida, T. Yamaguchi and K. Tanabe, Chem. Lett. (1988) 1869.
[10] J.-M. Herrman, J. Disdier and P. Pichat, J. Chem. Soc. Faraday Trans. I, 77 (1981) 2815.
[11] J.A. Navío and G. Colón, Stud. Surf. Sci. Catal., 82 (1994) 721.
[12] J.B. Goodenough, in M. Schiavello (Ed.), Photoelectrochemistry, Photocatalysis and Photoreactors, NATO-ASI Ser. C, Vol. 146, Reidel, Dordrecht, 1985, p. 3.
[13] M. Anpo, Res. Chem. Intermed., 11 (1989) 67.
[14] J.A. Navío, M. Macías, G. Colón, P.J. Sánchez-Soto, V. Augugliaro and L. Palmisano, Appl. Surf. Sci., 81 (1994) 325.
[15] M. Schiavello, V. Augugliaro and L. Palmisano, J. Catal., 127 (1991) 332.
[16] V. Augugliaro, M. Schiavello and L. Palmisano, AIChE J., 37 (1991) 1096.
[17] V. Augugliaro, M. Schiavello and L. Palmisano, Coord. Chem. Rev., 125 (1993) 173.
[18] V. Augugliaro, L. Palmisano, M. Schiavello, A. Sclafani, L. Marchese, G. Martra and F. Miano, Appl. Catal., 69 (1991) 323.
[19] S.L. Murov (Ed.), Handbook of Photochemistry, Marcel Dekker, New York, 1973, p. 119.
[20] P.J. Sánchez-Soto, M.A. Avilés, G. Colón, M. Macías and J.A. Navío, J. Sol–Gel Technol., 2 (1994) 325.
[21] G.P. Panasyuk, G.P. Budova and V.B. Lazarev, J. Thermal Anal., 16 (1979) 441.
[22] T. Yamaguchi, T. Morita, T.M. Salama and K. Tanabe, Catal. Lett., 4 (1990) 1.
[23] S.P. Tandon and J.P. Gupta, Phys. Status Solidi, 38 (1970) 363.
[24] L. Brus, J. Phys. Chem., 90 (1986) 555.
[25] V. Augugliaro, V. Loddo, L. Palmisano and M. Schiavello, Proc. 1st Conference on Chemical and Process Engineering, Florence (Italy) 13–15 May 1993, p. 783.
[26] V. Augugliaro, V. Loddo, L. Palmisano and M. Schiavello, J. Catal., 153 (1995) 32.
[27] R.I. Bickley, T. González-Carreño, J.S. Lees, L. Palmisano and R.J.D. Tilley, J. Solid State Chem., 92 (1991) 178.
[28] M. Fox, H. Ogawa and P. Pichat, J. Org. Chem., 54 (1989) 3847.